Current Crowding in Nanoscale Superconductors within the Ginzburg-Landau Model

Mattias Jönsson,[1] Robert Vedin,[1] Samuel Gyger,[2] James A. Sutton,[2] Stephan Steinhauer,[2]
Val Zwiller,[2] Mats Wallin,[1] and Jack Lidmar[1,*]

[1] *Department of Physics, KTH Royal Institute of Technology AlbaNova University Center, Stockholm SE 106 91, Sweden*

[2] *Department of Applied Physics, KTH Royal Institute of Technology AlbaNova University Center, Stockholm SE 106 91, Sweden*

The current density in a superconductor with turnarounds or constrictions is nonuniform due to a geometrical current-crowding effect. This effect reduces the critical current in the superconducting structure compared to a straight segment and is of importance when designing superconducting devices. We investigate the current-crowding effect in numerical simulations within the generalized time-dependent Ginzburg-Landau (GTDGL) model. The results are validated experimentally by measuring the magnetic field dependence of the critical current in superconducting-nanowire structures, similar to those employed in single-photon detector devices. Comparing the results with London theory, we conclude that the reduction in critical current is significantly smaller in the GTDGL model. This difference is attributed to the current redistribution effect, which reduces the current density at weak points of the superconductor and counteracts the current-crowding effect. We numerically investigate the effect of the fill factor on the critical current in a meander and conclude that the reduction of the critical current is low enough to justify fill factors higher than 33% for applications where the detection efficiency is critical. Finally, we propose a meander design that can combine a high fill factor and low current crowding.

I. INTRODUCTION

Mesoscale and nanoscale superconductors play a central role in contemporary device configurations applied in various research fields. Inhomogeneous current-density distributions, often termed current crowding, can occur at geometrical features such as corners, bends, and constrictions and severely impact the device properties of microwave resonators, filters, and waveguides. Another prominent example is superconducting-nanowire structures, which are the crucial building block for realizing devices capable of detecting light at the single-photon level [1]. Due to their outstanding performance in terms of detection efficiency, time resolution, and low intrinsic dark-count rates, superconducting-nanowire single-photon detectors (SNSPDs) have found widespread applications in, for instance, quantum optics, light detection and ranging (LIDAR), biological imaging, and astronomy [2–4]. Furthermore, SNSPDs can be embedded in photonic integrated circuits [5,6], which allows for miniaturized implementations of complex quantum-information-processing architectures. In general, the detection mechanism of SNSPDs [7] relies on operating the device relatively close to its critical current, to enable the transduction of single-photon absorption events into an electrical signal at high quantum efficiency. Hence, for further optimization of superconducting detectors and, more generally, of superconducting device properties, it is necessary to understand and mitigate the impact of current crowding, as the latter most commonly limits the critical current and the device functionality.

Current-crowding effects in superconducting-nanowire structures have previously been reported for the case of nanowire meanders with high fill factors [8] and attributed to inhomogeneous current distributions at the bends within the London model [9]. Moreover, the importance of the geometry on the critical current [10,11] and on the observed dark counts during SNSPD operation [12] has been highlighted. The application of magnetic fields has been proposed for probing and counteracting critical-current reduction due to crowding at nanowire bends using time-dependent Ginzburg-Landau simulations

---

*[*]jlidmar@kth.se

[13]. Several experiments have demonstrated an asymmetric critical current with respect to a reversal of the direction of an applied magnetic field perpendicular to the plane of the nanowire device [14–16]. To provide guidance for further device-design optimization, it is essential to benchmark different theoretical models related to inhomogeneous supercurrent distributions, explore their limitations, and validate them with experimental data.

This paper focuses on the nanowire hairpin, the basic building block of superconducting meanders, made up from a single 180° bend connected to two leads. The generalized time-dependent Ginzburg-Landau (GTDGL) model is used to investigate the effect of the inner-bend geometry on the critical current. To verify the simulations, the effect of an applied magnetic field on the critical current of such superconducting-nanowire structures is experimentally measured. Our results within the GTDGL model differ from those obtained with the London model, demonstrating that the latter significantly overestimates the impact of current crowding on the critical current in nanoscale superconductors. Hence, our results provide guidance for geometrical device design to achieve nanostructures with current-carrying capabilities close to the material limits.

The paper is organized as follows. In Sec. II, the current-crowding effect in the Ginzburg-Landau model is studied for the simple case of an annulus disk geometry and compared with the London model. In Sec. III, the theoretical model and the numerical methods used to simulate various hairpin geometries are described. In Sec. IV, the fabrication and experimental setup are presented. In Sec. V A, simulations and experimental results for the critical-current dependence on the applied magnetic field are presented. In Sec. V B, the current-crowding effects in the GTDGL and London models are compared for various hairpin geometries. In Sec. V C, the critical-current dependence on the fill factor is studied and in Sec. V D we suggest a meander geometry to mitigate current crowding. Finally, Sec. VI gives a summary and discussion of the results.

II. CURRENT CROWDING IN THE LONDON AND GINZBURG-LANDAU MODELS

The supercurrent density is given by $\mathbf{J} \propto |\psi|^2(\nabla\theta - \mathbf{A})$, where $\psi = |\psi|e^{i\theta}$ is the complex order parameter. In the London limit, the amplitude $|\psi|$ is assumed to be constant and in the absence of vortices the phase θ is single valued. If magnetic field fluctuations are neglected, formally by letting the London penetration depth $\lambda \to \infty$, the current pattern is described by an incompressible potential flow $\mathbf{J} \propto \nabla\theta$, with $\nabla \cdot \mathbf{J} \propto \nabla^2\theta = 0$.

The current-crowding effect has been thoroughly studied in Ref. [9] in the potential flow limit using the London model. By using conformal mapping techniques to compute the energy barrier for vortex crossings, it has been

concluded that a turnaround or a constriction results in a reduced critical current compared to a straight superconductor. Computation of the vortex barrier to find the critical current for a general superconducting geometry is difficult but it is possible to simplify the calculations when the smallest radius of curvature R is much larger than the coherence length ξ, which is often the case in practical applications. In this case, the critical current is obtained when the local critical-current density is reached somewhere in the superconductor. It is therefore sufficient to solve the Laplace equation to find the critical current.

In Ref. [9], it is shown that most 180° turnarounds result in a significant critical-current reduction and, in general, that sharper turnarounds tend to result in a larger reduction. It is also shown that there exists an optimal turnaround geometry that does not reduce the critical current compared to a straight superconductor, within London theory. The inner boundary of the optimal bend is, for $x \leq (2W/\pi)\ln 2$, parametrized as $y_\pm(x) = \pm(2W/\pi)\cos^{-1}[\exp{(\pi x/2W)}/2]$ (see Fig. 10 in Ref. [9]), which takes the limiting value $y_\pm = \pm W$ far from the bend. This means that two meander lines must be separated by a distance of $2W$ in order to use this design. The optimal turnaround geometry is thus ideal in terms of current crowding. A drawback is that the fill factor, defined as the fraction of area covered by the superconducting film, is limited to 33%.

The validity of the London model is limited to small currents well below I_c. Currents close to the critical current are outside this regime and hence results from the London model do not necessarily apply. This motivates the study of the reduction of the critical current due to the current-crowding effect in the Ginzburg-Landau model, which remains valid close to the critical current.

To clearly demonstrate the differences in the current-crowding effect in the Ginzburg-Landau model compared to the London model, we consider a superconducting disk geometry given by the annulus between two concentric circles. The width is W, the thickness d, the inner radius a, the coherence length ξ, and the Ginzburg-Landau parameter $\kappa \to \infty$, as depicted in Fig. 1(a). The cylindrical symmetry of this geometry may be used to simplify the time-independent Ginzburg-Landau model,

$$0 = (\nabla - i\mathbf{A})^2\psi + (1 - |\psi|^2)\psi, \quad (1)$$

into a nonlinear ordinary differential equation by assuming that the superconducting order parameter $\psi = |\psi|(r)e^{i\theta(\varphi)}$, where r and φ are cylindrical coordinates. Dimensionless units are used, as defined in Sec. III. The resulting ordinary differential equation is

$$0 = r^2\frac{\partial^2|\psi|}{\partial r^2} + r\frac{\partial|\psi|}{\partial r} + (r^2 - k^2)|\psi| - r^2|\psi|^3, \quad (2)$$
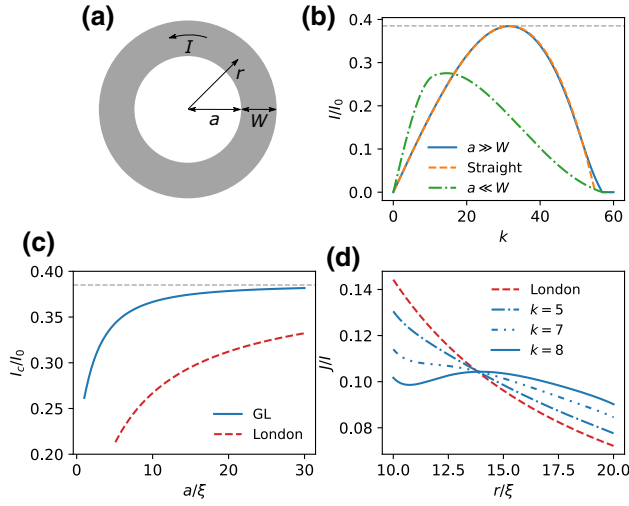
FIG. 1. The current-crowding effect in the Ginzburg-Landau model for an annulus area between concentric circles. (a) The geometry with inner radius a and width W used in the calculation. A current I is induced into the superconductor (gray) by setting k [see discussion below Eq. (2)]. (b) The current as a function of the applied flux (blue curve) for inner radius $a = 50\xi$ and width $W = 10\xi$. In the limit $a \gg W$, the geometry may be approximated with a straight superconductor and the analytical result from Eq. (3) provides excellent agreement (dashed orange curve). For $a = 10\xi$ and $W = 50\xi$ (dash-dotted green curve), the current-crowding effect is non-negligible and the critical current is reduced below $I_{\text{dep}} = 0.385I_0$. (c) The critical current as a function of the inner radius when $W = 10\xi$. The Ginzburg-Landau model (blue curve) predicts significantly higher critical currents compared to the London model (dashed red curve). The critical current is only evaluated for $a/\xi \geq 5$ in the London model due to complications when a is comparable to ξ [9]. (d) The current density along a radial cross section for the London model (dashed red curve) and the Ginzburg-Landau model (blue curves: dashed-dotted, $k = 5$; dashed-double-dotted, $k = 7$; solid, $k = 8$).

where $\theta(\varphi) = n\varphi$. A circulating current may be induced by threading a thin flux tube through the ring or by setting a nonzero winding number n of the phase, so that $k = n - \Phi/\Phi_0$, where Φ_0 is the flux quantum. Isolating boundary conditions are used on the superconductor-vacuum interface, i.e., $\partial|\psi|/\partial r = 0$. From the numerical solution of Eq. (2), the supercurrent density is obtained as $J(r) \propto |\psi|^2(\nabla\theta - \mathbf{A}) = k|\psi|^2/r$.

Figure 1(b) shows the calculated current $I = d\int_a^{a+W} J(r)dr$ in units of $I_0 = \hbar Wd/2\mu_0 e\lambda^2\xi$ as a function of k. As can be seen, there is a maximal current that can be sustained by a cylindrically symmetric solution. Higher currents necessarily break the symmetry by the nucleation of vortices that start to cross the wire and lead to dissipation in the system. For a geometry with a large inner radius compared to the width $a/W \gg 1$, the critical current equals the depairing current $I_{\text{dep}} = 2I_0/\sqrt{27} \approx 0.385I_0$ and the

curve is well approximated by the formula for a straight superconductor [17],

$$I = I_0 \frac{k}{k_0}\left(1 - \frac{k^2}{k_0^2}\right), \tag{3}$$

where the superfluid velocity $v_s \propto k$ and k_0 is a normalization factor that sets the maximal current at $k = k_0/\sqrt{3}$. For a smaller ratio of a/W, the critical current is less than the depairing current I_{dep} and thus demonstrates a non-negligible current-crowding effect.

In Fig. 1(c), results for the critical current (normalized to I_0) as a function of the inner radius are compared for the Ginzburg-Landau and London models. In general, the critical current is significantly higher in the Ginzburg-Landau model compared to the London model, which shows that the current-crowding effect is less pronounced than previously reported in the literature. This qualitative difference between the models is caused by the current redistribution effect, which is shown in Fig. 1(d). For sufficiently large k, the current density near the inner boundary is large enough to cause a significant suppression of the superconducting order parameter $|\psi|$. This suppression in turn limits the current density locally, which forces the current to redistribute. This results in a flatter current profile with smaller peak values, which increases the critical current and therefore weakens the current-crowding effect compared to the London limit.

III. THEORETICAL MODEL

To study the current-crowding effect in a general geometry, we consider a superconductor with a thickness d much smaller than the London penetration depth λ—i.e., $d \ll \lambda$—and a width W much smaller than the Pearl length $\Lambda = 2\lambda^2/d$, i.e., $W \ll \Lambda$. This is typically relevant for materials and device dimensions used in superconducting quantum circuits and detectors. In this regime, the magnetic field from the current passing through the superconductor has little influence on the magnetic field dynamics [9] and it is justifiable to take the Ginzburg-Landau parameter $\kappa = \lambda/\xi \to \infty$ and make the approximation that the magnetic field B is constant, normal to the superconducting surface, and equal to the applied magnetic field.

To simulate the superconductor, we employ the GTDGL model [18–20],

$$\frac{u}{\sqrt{1 + \gamma^2|\psi|^2}}\left(\frac{\partial}{\partial t} + i\mu + \frac{\gamma^2}{2}\frac{\partial|\psi|^2}{\partial t}\right)\psi$$
$$= (1 - |\psi|^2)\psi + (\nabla - i\mathbf{A})^2\psi, \tag{4}$$

$$\nabla^2\mu = \nabla \cdot \text{Im}[\psi^*(\nabla - i\mathbf{A})\psi], \tag{5}$$

$$\mathbf{A} = \frac{-By}{2}\hat{\mathbf{x}} + \frac{Bx}{2}\hat{\mathbf{y}}, \tag{6}$$

where ψ is the superconducting order parameter, $\mathbf{A}$ is the vector potential, and μ is the electric potential. We make a conventional choice for the material parameter $u = 5.79$ [18] and assume that $\gamma = 10$. The dimensionless units are chosen such that distances are measured in the coherence length ξ, time is measured in $\tau = \mu_0 \sigma \lambda^2$, where σ is the conductivity, voltages are measured in $v_0 = \hbar/2e\mu_0\sigma\lambda^2$, currents are measured in $J_0 = \hbar/2\mu_0 e\lambda^2\xi$, and magnetic fields are measured in $B_{c2} = \hbar/2e\xi^2$. Equation (6) is a result of the approximation that the magnetic field is constant and equal to the applied magnetic field B.

We simulate the GTDGL model for geometries such as the turnaround presented in Fig. 2(a). The superconductor is coupled to two metal terminals with opposite normal-current densities J_{ext} that control the current flowing through the superconductor. This is modeled by applying the boundary conditions $\psi = 0$ and $\hat{\mathbf{n}} \cdot \nabla\mu = J_{\text{ext}}$ on the superconductor-metal interfaces. The remaining boundaries are superconductor-vacuum interfaces and the boundary conditions are given by $\hat{\mathbf{n}} \cdot (\nabla - i\mathbf{A})\psi = 0$ and $\hat{\mathbf{n}} \cdot \nabla\mu = 0$ to ensure that no supercurrent or normal current flows across the boundary.

We solve the GTDGL given in Eqs. (4) and (5) using a finite-volume method on an unstructured Delaunay triangulation [21,22], where the edge lengths in the triangles are

at most $\xi/2$. Link variables are used for the magnetic vector potential $\mathbf{A}$ by introducing $U = \exp\left(-i\int \mathbf{A} \cdot d\mathbf{l}\right)$ and rewriting the covariant derivative as

$$(\nabla - i\mathbf{A})\psi = U^*\nabla(U\psi). \qquad (7)$$

This formulation of the covariant derivative preserves the gauge invariance when discretized on a lattice [23]. The electrical scalar potential μ is treated similarly for the covariant time derivative. The discretized form of Eq. (4) is solved using a semi-implicit Euler method and Eq. (5) is solved with a sparse lower-upper factorization.

IV. EXPERIMENTAL SETUP

Device fabrication is performed on silicon substrates covered with thermal SiO_2, relying on a room-temperature reactive-sputtering process of $Nb_xTi_{1-x}N$ with stoichiometry optimized for single-photon detectors [24]. The $Nb_xTi_{1-x}N$ thin films (thickness 9 nm) are patterned into nanowire structures via electron-beam lithography and reactive-ion etching. The SNSPDs consist of hairpins with a width of $W = 70$ nm and a fill factor of 33% ($U = 140$ nm). The leads are 50 μm long and connected to a lumped-element inductor to avoid latching. The detectors are mounted inside a closed-cycle dipstick system (Attodry 2100) with He exchange gas at temperatures below 2 K inside a uniaxial field created by a superconducting magnet and connected to coaxial cables leading to room temperature. The SNSPDs are operated using commercial control electronics (Single Quantum Atlas) containing a bias tee and a two-stage room-temperature amplifier. The measurement sweeps are controlled using PYTHON and the critical currents are extracted by fitting a step function using LMFIT [25]. The measurement configuration is schematically depicted in Fig. 2(a), whereas representative scanning-electron-microscopy (SEM) images of the investigated devices are presented in Fig. 2(b). This device design is immediately relevant for waveguide-integrated superconducting single-photon detectors employed in nanophotonic circuits [26].

V. RESULTS

A. Critical-current dependence on applied magnetic field

An applied perpendicular magnetic field will, depending on direction, either increase or decrease the amount of current crowding at the inner bend of a turn. This will then change the energy barrier for vortex crossings and lead to a lower or higher critical current of the structure and will show up as an asymmetry in $I_c(B)$ about zero field. For practical applications with both left and right bends, a homogeneous magnetic field could reduce the current crowding only at one type of bend. Still, from an experimental viewpoint, this is a useful diagnostic of current
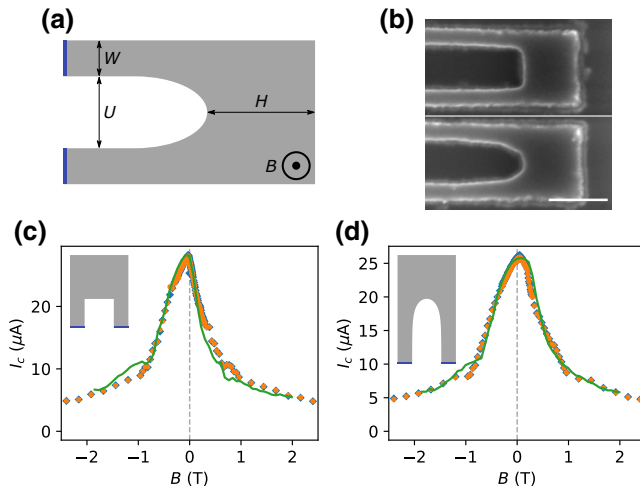

FIG. 2. (a) A typical turnaround used in the simulations. A uniformly distributed current density J is injected through the lower metal contact (blue) and the current flows through the superconductor (gray) to the upper metal contact. The leg width is $W = 14\xi$, the head width $H = 3W$, and U varies based on the fill factor. (b) A scanning-electron-microscopy (SEM) image of a hairpin device with a square and optimal turnaround. The scale bar is 200 nm. (c),(d) The experimentally measured critical current as a function of the magnetic field (blue diamond) fitted with simulation data (green curve) for a 33%-fill-factor (c) square and (d) optimal turnaround (shown in the insets). The experimental data for a reversed current direction and a reversed magnetic field (orange circle) overlap the positive current data (blue diamond).

crowding in hairpin geometries as studied here, since it relies on comparing the critical current in the same device at different fields, rather than different devices with varying geometries, which are susceptible to sample-to-sample variations.

The critical-current dependence on the applied magnetic field is investigated in both experiment and simulation by extracting critical currents from I-V curves for different constant applied fields. The results from experimental devices with fitted simulation data for the square turnaround and the optimal turnaround are presented in Figs. 2(c) and 2(d), respectively. To fit the simulation data, dimensions are reintroduced to the current by multiplying with $I_0 = WdJ_0$ and to the magnetic field by multiplying with B_{c2}. We also add an empirical constant offset B_{off} to the simulated magnetic field. The best fit corresponds to $B_{c2} = 10$ T, $B_{off} = 70$ mT, $I_0 = 75$ μA for the device with the square turnaround and $I_0 = 67$ μA for the optimal turnaround. These values correspond to the estimated parameters $\xi \approx 5.7$ nm and $\lambda \approx 600$ nm for $T \approx 2$ K. Extrapolation to $T = 0$ using BCS theory gives $\xi(0) \approx 5.1$ nm and $\lambda(0) \approx 550$ nm [17]. These are consistent with previously reported values for $Nb_xTi_{1-x}N$ films [27,28]. The assumed magnetic offset B_{off} moves the simulation-data peak slightly closer to zero magnetic field and is needed for a good fit. The origin of the offset is not known. However, it is unlikely that it is due to the presence of a constant magnetic field background, as shown by the overlapping data points in Figs. 2(c) and 2(d). In the literature, a stronger peak asymmetry has been reported [14–16], which motivates further study.

The simulation results in Figs. 2(c) and 2(d) are in good agreement with the experimental data, showing a larger asymmetry for the geometry with sharp corners. In a region around $B = -1$ T, the simulations display a bump that is not present in the experimental results. The bump seen in the simulation data has previously been reported in Refs. [13,15,29] and is attributed to the formation of a vortex lattice. The precise shape and location of bumps in this regime is likely to depend on the detailed geometry of the device. One possible explanation for the missing bumps in the experimental data shown in Figs. 2(c) and 2(d) is that vortices move more freely for nonzero temperatures. Another difference between experiment and simulation is present for the square turnaround when a positive magnetic field is applied, i.e., the simulation predicts a smaller critical current compared to experiment. This difference is likely explained by the 90° corners being rounded in the experimental device, as seen in the upper SEM image in Fig. 2(b).

Figure 3(a) shows the simulated critical current versus the magnetic field for different geometries: straight, circle, ellipse with aspect ratio 1 : 2, square, and optimal according to London theory. As expected from the symmetry of the straight superconducting strip, its critical current is
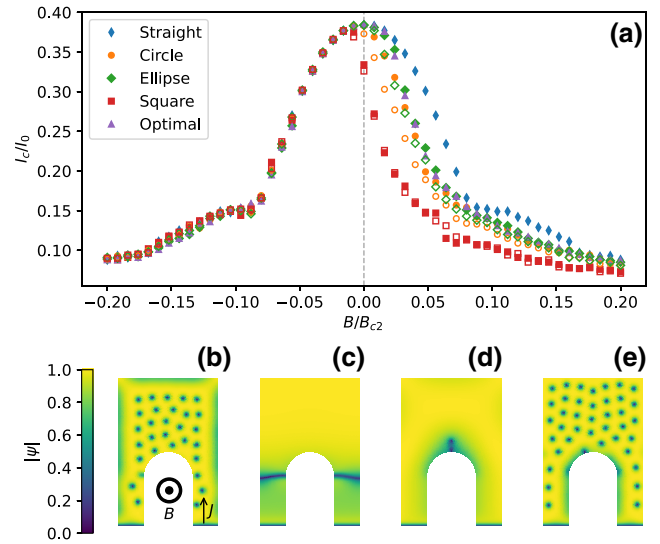

FIG. 3. Simulation results from the GTDGL model. (a) The simulated critical current as a function of the applied magnetic field for geometries with a 33% fill factor (filled markers) and a 50% fill factor (hollow markers). A straight superconducting strip (blue diamonds) is added as a current-crowding-free reference. (b)–(e) The superconducting order parameter, showing the breakdown mechanics slightly above I_c. A uniform current density enters the right leg and flows to the left leg. The positive magnetic field direction is toward the reader. (b) $B/B_{c2} = -0.1$. Vortices nucleate on the outer boundary and move across the nanowire. (c) $B/B_{c2} = 0$. Vortices nucleate at the start of the inner bend and create a phase-slip line. (d) $B/B_{c2} = 0.025$. Vortices nucleate at the tip of the turnaround. (e) $B/B_{c2} = 0.1$. Vortices nucleate on the inner bend and leave the superconductor on the outer boundary.

symmetric around $B = 0$. For the remaining geometries, the critical current is asymmetric around $B = 0$. As discussed, this asymmetry is a clear sign of current crowding being influenced by the screening currents induced by the applied magnetic field.

For sufficiently strong negative magnetic fields, the critical currents of the turnaround geometries coincide with the straight geometry, which is explained by the weakest point being located on the legs. This is shown in Fig. 3(b), where it is seen that the first nonstationary vortices nucleate on the outer boundary of the legs and flow inward toward the inner boundary. For zero magnetic field, all smooth geometries at 33% fill factor have a negligible reduction in the critical current, which is consistent with Fig. 3(c), where the weakest point is at the start of the inner bend. For small positive magnetic fields around $B/B_{c2} = 0.05$, the critical current is reduced compared to the straight geometry, which shows that the magnetic field aggravates the current-crowding effect. This is seen in Fig. 3(d), where the weakest point has moved to the tip of the turnaround as a result of current crowding. For a

sufficiently strong positive magnetic field, the critical currents for the turnarounds approach the value for the straight geometry. In Fig. 3(e), nonstationary vortices nucleate everywhere on the inner boundary, which suggests that the inner bend is less limiting for the critical current.

B. Current crowding in GTDGL versus London

In Sec. II, we show that the current-crowding effect in the Ginzburg-Landau model is qualitatively different compared to the London model when considering a system of concentric circles. The difference between the models is that Ginzburg-Landau takes the suppression of the superconducting order parameter into account, which results in a redistribution of the current density. The current redistribution effect depends on the turnaround geometry and we therefore investigate different geometries.

In the GTDGL model, we define the critical current as the current at which vortices start to flow across the wire, since the vortex motion will generate a voltage. In the London model, we define the critical current at which the vortex barrier for crossings is zero. For a bend with a radius of curvature R much larger than ξ, this will coincide with the current when the critical-current density is locally reached somewhere [9]. For simplicity, the comparison is restricted to geometries such that $R \geq 10\xi$ by scaling up the size if necessary [30].

In Fig. 4, the reduction of the critical current is compared between the GTDGL model and the London model for the different geometries. All geometries, except for the optimal geometry, display significantly smaller reduction in the GTDGL model compared to the London model. This shows that the London model overestimates the impact of current crowding and turnaround geometry. From the GTDGL simulations, we may therefore conclude that for sufficiently wide heads [large H in Fig. 2(a)], the exact shape of a rounded inner bend does not significantly affect the critical current for fill factors up to 50%. Defects in the manufacturing process may be a larger contribution to the reduction than the geometrical form of the inner bend.

C. Critical-current dependence on fill factor

Figure 5(a) shows the critical-current reduction as a function of the fill factor for the GTDGL simulations. The fill factor is tuned for each geometry by changing the spacing between the legs U while keeping $W = 14\xi$ fixed [see Fig. 2(a)] and rescaling the inner bend to leave the geometry unchanged. The critical current decreases as the fill factor increases, which is expected since the current-crowding effect becomes stronger for sharper turnarounds. The numerical results for the critical current of the rounded geometries display a reduction similar to that of the experimental results in Ref. [8]. The latter were based on devices with square inner bends that tend to be rounded due to
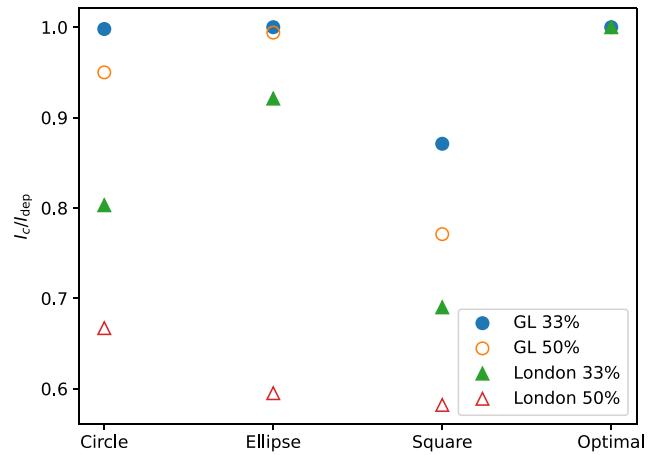
FIG. 4. Reduction of the critical current compared to a straight superconductor. The reductions predicted by the GTDGL model with a 33% fill factor (blue circle) and a 50% fill factor (orange hollow circle) are compared with the London model for a 33% fill factor (green triangle) and a 50% fill factor (red hollow triangle). All geometries are rescaled such that the smallest radius of curvature $R \geq 10\xi$, which allows for direct comparison between the GTDGL and London models without any extra compensation factors due to small geometries. The width W is 14ξ for circle 33%, 20ξ for circle 50%, 20ξ for ellipse 33%, 40ξ for ellipse 50%, 14ξ for square 33%, and 20ξ for square 50%. For all geometries except for the optimal, the London model predicts a significantly larger reduction of the critical current than the GTDGL model.

fabrication limitations, which makes them more comparable to the rounded simulation geometries. Furthermore, the reduction in the critical current is less than what is expected from London theory, as has been seen experimentally in Refs. [31,32].

The shape of the inner bend plays a role in how quickly the critical current drops as the fill factor is increased. As a result, the best choice of inner bend may change as the fill factor increases. In the limiting case approaching 100% fill factor, it is clear that all radii of curvature are zero, all geometries have the same shape, and the critical currents are equal. Figure 5(a) can be used to determine a trade-off between the optical design for high detection efficiency [33] and the suppression of the critical current by varying the fill factor.

D. Meander with arbitrary fill factor and low current crowding

As shown in Sec. V C, the GTDGL simulations indicate that the critical current of the structure is not as sensitive to the geometry as previously reported. However, for high fill factors, the current-crowding effect still leads to a considerable reduction of the critical current. In the case of a standard meander composed of straight lines connected with 180° turnarounds, there is a trade-off between having
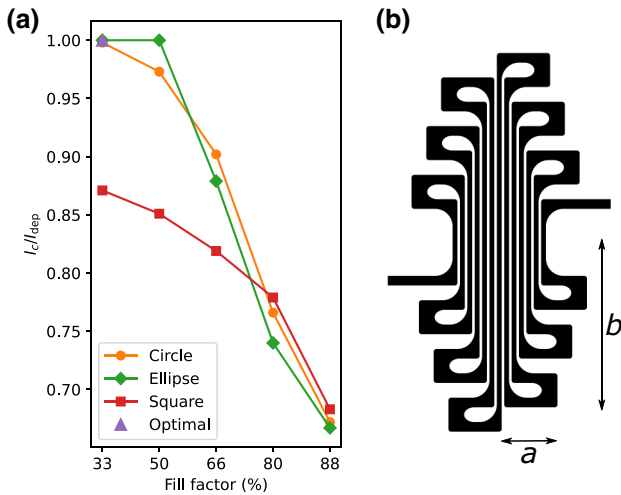
FIG. 5. (a) The reduction of the critical current compared to a straight superconductor as a function of the fill factor. For a 33% fill factor, the reduction of the critical current is negligible for all smooth turnarounds. The critical current is reduced as the fill factor increases and for an 88% fill factor all geometries converge to the same critical current. (b) An example of a meander with L bends used to minimize the current-crowding effect, while simultaneously allowing an arbitrary fill factor. The use of L bends results in a changed aspect ratio, with $a \neq b$.

a high critical current and a high fill factor. One possible solution is to increase the thickness of the superconducting film at the bends in order to locally reduce the current density [34].

We propose a meander design that eliminates the trade-off between the critical current and the fill factor while avoiding the need for a variable film thickness. The concept uses L bends, which are turnarounds consisting of an extra 90° turn before the 180° turnaround, as depicted in Fig. 5(b). This design allows the fill factor near the turnaround to be smaller than the fill factor of the light-detecting meander lines, which makes it possible to use an arbitrary fill factor while allowing the turnaround to be wider and have a low fill factor. The downside of this design is that the meander will be elongated due to the extra space required for the L bends and, in general, the ratio $b/a > 1$.

The ratio b/a may, for a large number of lines, be approximated as a ratio between the pitch in the L bend P_B and the pitch in the meander lines P_M. Alternatively, it can also be approximated using the fill factor of the L bend ff_B, the meander ff_M, and the ratio between the width of the superconducting wire in the bend and in the meander line $k = W_B/W_M$. Thus

$$\frac{b}{a} = \frac{P_B}{P_M} = k\frac{ff_M}{ff_B}. \tag{8}$$

In order to estimate the elongation of an L-bend meander, we consider the limiting case where the meander lines have width $W_M = W$ and a 100% fill factor, while the L bends have width $W_B = 2W$ to reduce dark counts and allow for a 33% fill factor. These dimensions gives $b = 6a$ and the meander area would increase by about a factor of 3 to cover the same circular area as a traditional meander.

Recently, the same idea has been independently proposed and experimentally realized for high-fill-factor superconducting microwire single-photon detectors in Ref. [35]. The resulting detectors combine high detection efficiency and low polarization sensitivity.

VI. SUMMARY

We use the GTDGL model (in the limit $\lambda \to \infty$) to explore the current-crowding effect in thin ($d \ll \lambda$) superconducting nanostructures with widths $W \gtrsim 14\xi$. This regime is relevant for superconducting quantum circuits and detectors, based on, for example, NbN and $\mathrm{Nb}_x\mathrm{Ti}_{1-x}\mathrm{N}$. The theoretical predictions are tested experimentally by comparing how the critical current varies with the applied magnetic field for two distinct nanowire turnaround geometries. In comparison to the previously used London model, we show that the reduction of the critical current due to current crowding is substantially less pronounced in the GTDGL model. This finding is explained by the suppression of the superconducting order parameter near bends, which causes current redistribution close to sharp turns. Within London theory, it is possible to design optimal turnarounds without current crowding but this restricts the fill factor to 33%. Using the more accurate description provided by the GTDGL model, our results show that it is possible to achieve less than 1% reduction for a 50% fill factor. We propose that this marked difference in predicted critical currents considerably loosens the design restrictions for a large range of superconducting nanodevices and circuits. Hence, our results may pave the way toward devices with improved performance and current-carrying capabilities approaching the material limits.

The simulation software is available on Ref. [36].

———

[1] G. Gol'tsman, O. Okunev, G. Chulkova, A. Lipatov, A. Dzardanov, K. Smirnov, A. Semenov, B. Voronov, C. Williams, and R. Sobolewski, Fabrication and properties of an ultrafast NbN hot-electron single-photon detector, IEEE Trans. Appl. Supercon. **11**, 574 (2001).

[2] R. H. Hadfield and G. Johansson, *Superconducting Devices in Quantum Optics* (Springer International Publishing, Cham, 2016).

[3] I. Holzman and Y. Ivry, Superconducting nanowires for single-photon detection: Progress, challenges, and opportunities, Adv. Quantum Technol. **2**, 1800058 (2019).

[4] I. Esmaeil Zadeh, J. Chang, J. W. N. Los, S. Gyger, A. W. Elshaari, S. Steinhauer, S. N. Dorenbos, and V. Zwiller, Superconducting nanowire single-photon detectors: A perspective on evolution, state-of-the-art, future developments, and applications, Appl. Phys. Lett. **118**, 190502 (2021).

[5] S. Ferrari, C. Schuck, and W. Pernice, Waveguide-integrated superconducting nanowire single-photon detectors, Nanophotonics **7**, 1725 (2018).

[6] G. Moody, *et al.*, Roadmap on integrated quantum photonics, J. Phys. Photon. **4**, 012501 (2021).

[7] A. Engel, J. Lonsky, X. Zhang, and A. Schilling, Detection mechanism in SNSPD: Numerical results of a conceptually simple, yet powerful detection model, IEEE Trans. Appl. Supercon. **25**, 2200407 (2015).

[8] J. K. W. Yang, A. J. Kerman, E. A. Dauler, B. Cord, V. Anant, R. J. Molnar, and K. K. Berggren, Suppressed critical current in superconducting nanowire single-photon detectors with high fill-factors, IEEE Trans. Appl. Supercon. **19**, 318 (2009).

[9] J. R. Clem and K. K. Berggren, Geometry-dependent critical currents in superconducting nanocircuits, Phys. Rev. B **84**, 174510 (2011).

[10] H. L. Hortensius, E. F. C. Driessen, T. M. Klapwijk, K. K. Berggren, and J. R. Clem, Critical-current reduction in thin superconducting wires due to current crowding, Appl. Phys. Lett. **100**, 182602 (2012).

[11] D. Henrich, P. Reichensperger, M. Hofherr, J. M. Meckbach, K. Il'in, M. Siegel, A. Semenov, A. Zotova, and D. Y. Vodolazov, Geometry-induced reduction of the critical current in superconducting nanowires, Phys. Rev. B **86**, 144504 (2012).

[12] M. K. Akhlaghi, H. Atikian, A. Eftekharian, M. Loncar, and A. H. Majedi, Reduced dark counts in optimized geometries for superconducting nanowire single photon detectors, Opt. Express **20**, 23610 (2012).

[13] J. R. Clem, Y. Mawatari, G. R. Berdiyorov, and F. M. Peeters, Predicted field-dependent increase of critical currents in asymmetric superconducting nanocircuits, Phys. Rev. B **85**, 144511 (2012).

[14] O.-A. Adami, D. Cerbu, D. Cabosart, M. Motta, J. Cuppens, W. A. Ortiz, V. V. Moshchalkov, B. Hackens, R. Delamare, J. Van de Vondel, and A. V. Silhanek, Current crowding effects in superconducting corner-shaped Al microstrips, Appl. Phys. Lett. **102**, 052603 (2013).

[15] K. Ilin, D. Henrich, Y. Luck, Y. Liang, M. Siegel, and D. Y. Vodolazov, Critical current of Nb, NbN, and TaN thin-film bridges with and without geometrical nonuniformities in a magnetic field, Phys. Rev. B **89**, 184511 (2014).

[16] I. Charaev, A. Semenov, R. Lusche, K. Ilin, H.-W. Huebers, and M. Siegel, Enhancement of critical currents and photon count rates by magnetic field in spiral superconducting nanowire single-photon detectors, IEEE Trans. Appl. Supercon. **26**, 2200304 (2016).1051-8223

[17] M. Tinkam, *Introduction to Superconductivity* (Dover, Mineola, N.Y., 1996), 110.

[18] L. Kramer and R. J. Watts-Tobin, Theory of Dissipative Current-Carrying States in Superconducting Filaments, Phys. Rev. Lett. **40**, 1041 (1978).

[19] R. J. Watts-Tobin, Y. Krähenbühl, and L. Kramer, Nonequilibrium theory of dirty, current-carrying superconductors: phase-slip oscillators in narrow filaments near T_c, J. Low Temp. Phys. **42**, 459 (1981).

[20] N. Kopnin, *Theory of Nonequilibrium Superconductivity* (Oxford University Press, Oxford, 2001), 215.

[21] Q. Du, R. A. Nicolaides, and X. Wu, Analysis and convergence of a covolume approximation of the Ginzburg-Landau model of superconductivity, SIAM J. Numer. Anal. **35**, 1049 (1998).

[22] Q. Du and L. Ju, Numerical simulations of the quantized vortices on a thin superconducting hollow sphere, J. Comput. Phys. **201**, 511 (2004).

[23] W. D. Gropp, H. G. Kaper, G. K. Leaf, D. M. Levine, M. Palumbo, and V. M. Vinokur, Numerical simulation of vortex dynamics in type-II superconductors, J. Comput. Phys. **123**, 254 (1996).

[24] J. Zichi, J. Chang, S. Steinhauer, K. von Fieandt, J. W. N. Los, G. Visser, N. Kalhor, T. Lettner, A. W. Elshaari, I. E. Zadeh, and V. Zwiller, Optimizing the stoichiometry of ultrathin NbTiN films for high-performance superconducting nanowire single-photon detectors, Opt. Express **27**, 26579 (2019).

[25] M. Newville, T. Stensitzki, D. B. Allen, and A. Ingargiola, LMFIT: Non-linear least-square minimization and curve-fitting for PYTHON. Zenodo (2014).

[26] S. Gyger, J. Zichi, L. Schweickert, A. W. Elshaari, S. Steinhauer, S. F. C. da Silva, A. Rastelli, V. Zwiller, K. D. Jöns, and C. Errando-Herranz, Reconfigurable photonics with on-chip single-photon detectors, Nat. Commun. **12**, 1408 (2021).

[27] M. Sidorova, A. D. Semenov, H.-W. Hübers, S. Gyger, S. Steinhauer, X. Zhang, and A. Schilling, Magnetoconductance and photoresponse properties of disordered NbTiN films, Phys. Rev. B **104**, 184514 (2021).

[28] D. J. Thoen, B. G. C. Bos, E. A. Haalebos, T. M. Klapwijk, J. J. Baselmans, and A. Endo, Superconducting NbTiN Thin Films with Highly Uniform Properties over a 100 mm Wafer, IEEE Trans. Appl. Supercon. **27**, 1 (2017).

[29] D. Y. Vodolazov, Vortex-induced negative magnetoresistance and peak effect in narrow superconducting films, Phys. Rev. B **88**, 014525 (2013).

[30] For the square geometries, we use a rescaling factor such that the spacing between the legs is much larger than the coherence length and use Eq. (100) in Ref. [9] to compute the reduction factors.

[31] Y. P. Korneeva, N. N. Manova, M. A. Dryazgov, N. O. Simonov, P. I. Zolotov, and A. A. Korneev, Influence of sheet resistance and strip width on the detection efficiency saturation in micron-wide superconducting strips and large-area meanders, Supercon. Science Technol. **34,** 084001 (2021).

[32] Y. Meng, K. Zou, N. Hu, X. Lan, L. Xu, J. Zichi, S. Steinhauer, V. Zwiller, and X. Hu, Fractal superconducting nanowire avalanche photodetector at 1550 nm with 60% system detection efficiency and 1.05 polarization sensitivity, Opt. Lett. **45,** 471 (2020).

[33] V. Anant, A. J. Kerman, E. A. Dauler, J. K. W. Yang, K. M. Rosfjord, and K. K. Berggren, Optical properties of superconducting nanowire single-photon detectors, Opt. Express **16,** 10750 (2008).

[34] R. Baghdadi, E. Schmidt, S. Jahani, I. Charaev, M. G. W. Müller, M. Colangelo, D. Zhu, K. Ilin, A. D. Semenov, Z. Jacob, M. Siegel, and K. K. Berggren, Enhancing the performance of superconducting nanowire-based detectors with high-filling factor by using variable thickness, Supercon. Science Technol. **34,** 035010 (2021).

[35] D. V. Reddy, N. Otrooshi, S. W. Nam, R. P. Mirin, and V. B. Verma, Broadband polarization insensitivity and high detection efficiency in high-fill-factor superconducting microwire single-photon detectors, APL Photon. **7,** 051302 (2022).

[36] https://github.com/afsa/super-detector-py.